

1 **Fire-precipitation interactions amplify the quasi-biennial**
2 **variability of fires over southern Mexico and Central America**

3 Yawen Liu ^{1,2}, Yun Qian ^{3*}, Philip J. Rasch ³, Kai Zhang ³, L. Ruby Leung³, Yuhang Wang ⁴,
4 Minghuai Wang ^{1,2}, Hailong Wang ³, Xin Huang^{1,2}, and Xiu-Qun Yang ¹

5 ¹School of Atmospheric Sciences, Nanjing University, China

6 ²Joint International Research Laboratory of Atmospheric and Earth System Sciences & Institute
7 for Climate and Global Change Research, Nanjing University, China

8 ³Pacific Northwest National Laboratory, Richland, Washington, USA

9 ⁴School of Earth and Atmospheric Sciences, Georgia Institute of Technology, Atlanta, Georgia,
10 USA

11 *Correspondence to:* Yun Qian (yun.qian@pnnl.gov)

12 **Abstract.** Fires have great ecological, social, and economic impacts. However, fire prediction and
13 management remain a challenge due to a limited understanding of their role in the Earth system.
14 Fires over southern Mexico and Central America (SMCA) are a good example, which greatly
15 impact local air quality and regional climate. Here we report that the spring-peak (Apr-May) fire
16 activities in this region have a distinct quasi-biennial signal based on multiple satellite datasets
17 measuring different fire characteristics. The variability is initially driven by the quasi-biennial
18 variations of precipitation. Composite analysis indicates that strong fire years correspond to
19 suppressed ascending motions and weakened precipitation over the SMCA. The anomalous
20 precipitation over the SMCA is further found to be mostly related to the East Pacific-North Pacific
21 (EP-NP) pattern two months previous to the fire season. The positive phase of EP-NP leads to
22 enhanced precipitation over the eastern US yet suppressed precipitation over SMCA, similar to the
23 spatial pattern of precipitation difference between strong and weak fire years. Meanwhile, the
24 quasi-biennial signals in precipitation and fires appear to be amplified by their interactions through
25 a positive feedback loop on short timescales. Model simulations show that in strong fire years,
26 more aerosol particles are released and transported downstream over the Gulf of Mexico and the
27 eastern US, where suspended light-absorbing aerosols warm the atmosphere and cause ascending
28 motions of the air aloft. Subsequently, a compensating downward motion is formed over the fire
29 source region and ultimately suppresses precipitation and intensifies fires. Statistical analysis
30 shows the different duration of the two-way interaction, where the fire suppression effect by
31 precipitation lasts for more than 20 days, while fire leads to a decrease in precipitation at shorter
32 time scales (3-5 days). This study demonstrates the importance of fire-climate interactions in
33 shaping the fire activities on interannual scale and highlights how precipitation-fire interactions at
34 short timescales contribute to the interannual variability of both fire and precipitation.

35 **1 Introduction**

36 Natural and human-induced fires are key features of the Earth system (Bowman et al., 2009).
37 Uncontrolled large fires damage biodiversity, affect human health, and incur high economic costs
38 (Knorr et al., 2017; Aguilera et al., 2021; Bowman et al., 2017). Comprehensive knowledge of
39 fires' causes, variability, and climate effects is necessary to accommodate or manage fires
40 effectively, and to mitigate adverse societal impacts.

41 Changes in climate alter fire regimes (Power et al., 2008; Jolly et al., 2015), because the occurrence
42 and intensity of fires depend on meteorological factors such as precipitation, wind, and humidity
43 (Flannigan et al., 2009; Marlon et al., 2008; Abram et al., 2021; Fang et al., 2021). Fires alter
44 weather and climate as well: they are important sources of aerosol particles that modify Earth's
45 energy and water budget either by directly absorbing and scattering sunlight or affecting cloud
46 microphysical processes (Voulgarakis and Field, 2015; Jiang et al., 2020; Liu et al., 2018; Yue et
47 al., 2022; Lu et al., 2018). There are many modes of interaction. The modes are complex, operate
48 through a variety of mechanisms, and manifest on a large variety of time and space scales (Ding
49 et al., 2021; Zhang et al., 2022). For example, Huang et al. (2023) have demonstrated that synoptic-
50 scale fire-weather feedback plays a prime role in driving extreme fires in the Mediterranean and
51 monsoon climate regimes over the US West Coast and Southeastern Asia. On interannual scales,
52 fires in the maritime subcontinent have been shown to affect SSTs, land temperature as well as
53 atmospheric stability, and influence ENSO on 3-6 year timescales (Tosca et al., 2010). The
54 extreme 2019-2020 Australian fires have also been demonstrated to contribute to the 2020-2022
55 strong La Niña event by enhancing cloud albedo, cooling and drying out the air, and forming a
56 positive feedback between the northward migration of intertropical convergence zone and sea
57 surface temperature cooling in the Niño3.4 region (Fasullo et al., 2023). Moreover, on even longer
58 timescales, fires can affect the accumulation of carbon dioxide and methane by modifying global
59 features like the Hadley circulation that change precipitation and temperature patterns and
60 eventually affect forest ecosystems to produce feedback operating over decades and centuries
61 (Crutzen and Andreae, 1990; Page et al., 2002; Tosca et al., 2013). It is hence necessary to explore
62 fire characteristics with special considerations of their multi-scale variability and feedback.

63 From a global perspective, fires occur progressively more frequently towards the tropics (Mouillot
64 and Field, 2005). Tropical savanna and forest burning contribute approximately 80% of global

65 open fire emissions (Bond et al., 2013). However, tropical regions also feature a great diversity of
66 climate-weather systems that affect fire occurrence and seasonality. In the tropical Northern
67 Hemisphere, fires over tropical southern Mexico and Central America (SMCA) occur during the
68 Feb-May dry season and peak in April-May (Magi et al., 2012). These fire activities have a
69 substantial influence on local air quality and human health (e.g., over Mexico City [19-20° N, 98-
70 100°W] and the Yucatan region (Crouse et al., 2009; Yokelson et al., 2007; Yokelson et al.,
71 2009). Fire emissions over the SMCA region also affect the eastern US after long-range transport
72 (Kreidenweis et al., 2001; Lee et al., 2006; Rogers and Bowman, 2001). Understanding the
73 processes that shape fire variabilities over this region is hence important locally (for air quality
74 and fire management) and over broader regions.

75 Here, for the first time, we report a distinct quasi-biennial variability of fire activities over the
76 southern Mexico and Central America region (SMCA, 10-25°N, 80-100°W) during the peak
77 burning months (April – May) over 2003-2019 by validating different fire characteristics with the
78 use of multiple independent datasets. We further explore the dominant causes of this quasi-biennial
79 signal and provide concrete evidence for positive fire-precipitation feedback on short timescales
80 to amplify the quasi-biennial signal based on model simulations.

81 **2 Data and Methods**

82 **2.1 Observations**

83 Two sets of fire emission inventories were used to investigate the interannual variability of fire
84 activities. The Global Fire Emissions Database with small fires version 4.1 (GFED v4.1s) is a
85 bottom-up inventory that generates fire-consumed dry matter using fire-burned areas combined
86 with emission factors (Giglio et al., 2013; Randerson et al., 2012). GFED v4.1s provides monthly
87 mean fire-consumed dry matter in total and for individual fire types at 0.25-degree spatial
88 resolution. The Quick Fire Emissions Dataset (QFED) is a top-down emission inventory that
89 generates fire emissions by using empirical relationships between fire-consumed dry matter and
90 fire radiative power (Koster et al., 2015). Daily emissions of fire-emitted species at 0.1 horizontal
91 resolution from QFED version 2.5 were examined. Since the interannual variations of different
92 species are consistent, only variation of fire-emitted black carbon (BC) is shown here. We focused
93 on the fire activities after 2003 to exclude the influence of the extremely strong ENSO events,

94 specifically the 1997/1998 El Niño event and the subsequent 1998-2000 La Niña event, which are
95 among the most powerful ENSO events in recorded history.

96 We also examined the interannual variation of fire-induced changes in aerosol optical depth based
97 on the MERRA-2 reanalysis data (Gelaro et al., 2017) and Level 3 version 4.2 CALIPSO satellite
98 dataset (Winker et al., 2013). For the MERRA-2 data, monthly mean BC aerosol optical depth
99 (AOD) was used for a better comparison with the BC emission from QFED emission data. The
100 CALIPSO product divides aerosol into six sub-types, and the gridded monthly mean 532nm AOD
101 for the biomass burning aerosol type under all-sky conditions was analyzed. We used the MODIS
102 version 6.1 gross primary productivity (GPP) product (MOD17A2H, (Running, 2021)), which
103 measures the growth of the terrestrial vegetation as a proxy for fuel load. A cumulative 8-day
104 composite of GPP values is provided with a 500m pixel size. The average of GPP in the month
105 (March) prior to the burning season is examined. Interannual variations in the shortwave diffuse
106 radiative fluxes at surface, which is closely related to photosynthesis rates and primary
107 productivity is also analyzed using the photosynthetically active radiation from the Earth's Radiant
108 Energy System (CERES) product (Su et al., 2007).

109 In order to investigate the climate influence on fire activities, we analyzed monthly mean
110 temperature and maximum temperature from the Climatic Research Unit gridded Time Series
111 (CRU TS) version 4.06 (Harris et al., 2014). The dataset is constructed based on station
112 observations and provides monthly data over the global land surface at 0.5-degree resolution. Apart
113 from the CRU dataset, two sets of satellite observations of precipitation were analyzed: the
114 monthly Integrated Multi-satellitE Retrievals for GPM (IMERG) precipitation estimates at 0.1
115 degrees (Huffman et al., 2015) and the 1-degree daily (version 1.3), 2.5-degree monthly
116 (version 2.3) Global Precipitation Climatology Project (GPCP) precipitation estimates (Adler et al.,
117 2018; Adler, 2017). IMERG is intended to intercalibrate and merge satellite microwave
118 precipitation estimates together with microwave-calibrated infrared satellite estimates and
119 precipitation gauge analyses (Huffman et al., 2020). Monthly mean 500hPa vertical velocity (ω)
120 at 2.5 degrees from NCEP/NCAR reanalysis (Kanamitsu et al., 2002) and 10m wind speed at 0.25
121 degrees from ERA5 reanalysis (Hersbach et al., 2020) were used in our work. We also calculated
122 near surface relative humidity and vapor pressure deficit following Chiodi et al. (2021) with the
123 use of 2m temperature and dew point temperature from ERA5 reanalysis data. In order to

124 understand the interannual variation of precipitation, we examined the relationship between
125 precipitation and ten different teleconnection patterns, including Atlantic Meridional Mode
126 (AMM), East Pacific/North Pacific Oscillation (EP/NP), ENSO, North Atlantic Oscillation
127 (NAO), North Tropical Atlantic index (NTA), Pacific North American index (PNA), Tropical
128 Northern Atlantic index (TNA), Tropical Southern Atlantic index (TSA), Western Hemisphere
129 warming pool (WHWP), Quasi-biennial Oscillation (QBO). These indices and their detailed
130 definitions can be obtained from <https://psl.noaa.gov/data/climateindices/list/>.

131 **2.2 Model experiment**

132 The CESM2.1.0 model with the Community Atmosphere Model version 6 (CAM6) (Danabasoglu
133 et al., 2020) was used to investigate the feedback of fire-emitted aerosols on precipitation. The
134 F2000 component set was used with the prescribed sea surface temperature in the year 2000. The
135 horizontal resolution is set as 0.9-degree latitude by 1.25-degree longitude with 32 vertical levels.
136 Two groups of simulations were conducted. Each was driven by the representative fire emissions
137 in strong and weak fire years and referred to as Case_Strong and Case_Weak. The difference in
138 variables (e.g., temperature and precipitation) between the two cases (Case_Strong minus
139 Case_Weak) indicate the influence, or difference in feedback, caused by stronger fire emissions.
140 As our work focused on the influence of fire activities over SMCA, only fire emissions over the
141 SMCA region were considered. Since fire emissions and anthropogenic emissions are specified
142 separately in the CESM2 model, we modified the default fire emission inventory (Van Marle et
143 al., 2017) in CESM2.1.0 accordingly while global anthropogenic emissions were kept unchanged
144 and remained the same between cases. Given that composite analysis indicates fire emissions in
145 weak fire years are approximately half those in strong fire years. We simply used the average of
146 fire emissions during strong fire years in Case_Strong, and reduced these by half in Case_Weak.
147 More subtle changes in fire locations between strong and weak fire years are hence ignored.
148 Furthermore, global climate models have long been found to underestimate fire-induced changes
149 in aerosols (Zhong et al., 2022). Hence, in order to ensure the simulated difference in fire-induced
150 AOD between Case_Strong and Case_Weak is comparable to observations, the default inventory
151 is multiplied by a factor of 3 to ensure the simulated fire-induced AOD changes are comparable to
152 observations. For each group, 9 ensemble simulations were performed with slight differences in
153 their initial conditions. The ensemble mean is calculated as the average of 9 members. All

154 simulations start on Jan.1 with a 3-month spin-up time. The T-test is used to identify statistically
155 significant differences between Case_Strong and Case_Weak.

156 **3 Results**

157 **3.1 Biennial variability of fire activities**

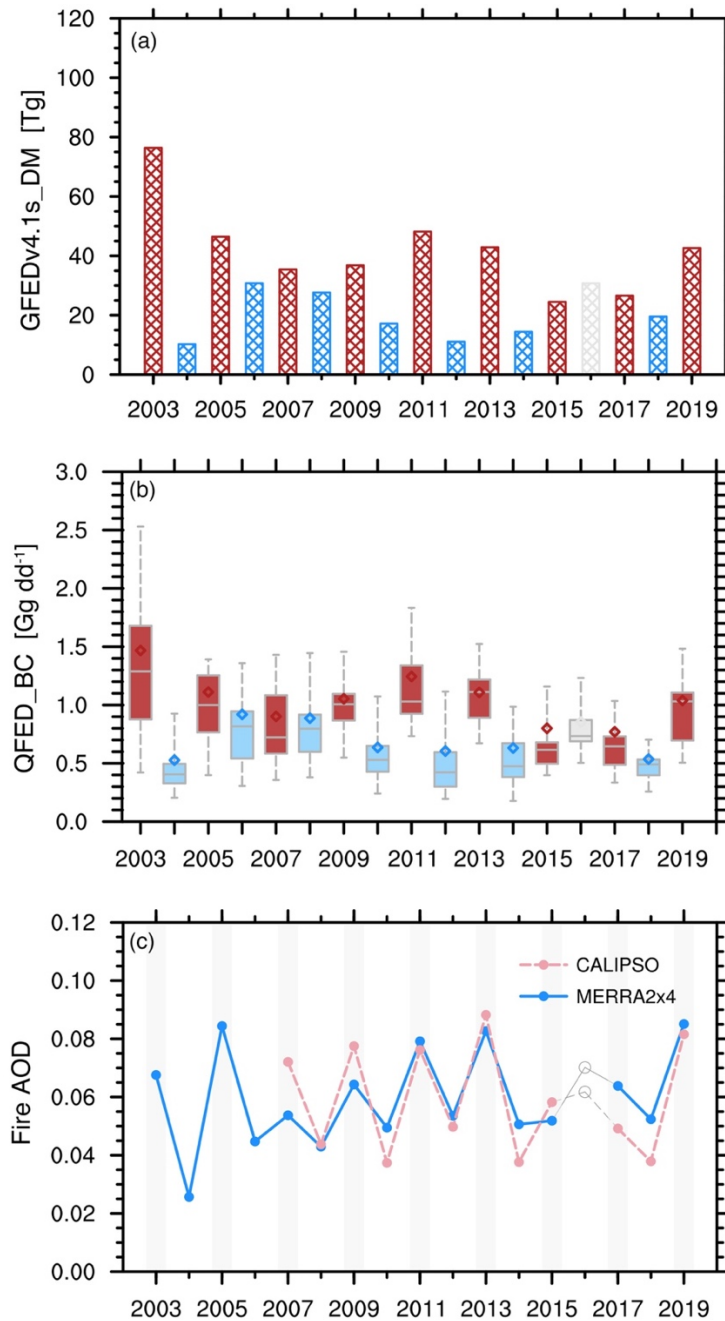
158 We focus on the southern Mexico and Central America region (SMCA) covering both the Yucatan
159 region and Mexico City. Major fire types in this region consist of deforestation fires, savanna fires,
160 and agricultural waste burning, which respectively are estimated to consume 45.5%, 42.1%, and
161 12.40% of the total burned dry matter during the peak burning months (Apr-May) of the 17-year
162 (2003-2019) study period.

163 As shown in Fig. 1a, GFEDv4.1s estimates of the regional sum of the total dry matter consumed
164 by fire activities feature obvious quasi-biennial variability. Generally speaking, fire activities in
165 odd-numbered years show higher consumption of dry matter than adjacent even-numbered years
166 with the only exception of the year 2016, which might be related to a long-lasting El Niño event
167 spanning 2014-2016. Composites of fire consumption of dry matter indicate enhanced fire
168 activities along both sides of the high terrains in odd-numbered years, and the most profound
169 difference appears over the bordering area between southern Mexico and Guatemala (Fig. S2). The
170 average fire-consumed dry matter here differs by more than a factor of 6 between odd-numbered
171 and even-numbered years.

172 The quasi-biennial variability of fire activities is also evident when examining fire emissions of
173 typical fire-emitted species based on the QFED inventory (Fig. 1b). Similarly, fire-emitted BC in
174 odd-numbered years is higher than those in the adjacent even-numbered years, when considering
175 both regional mean and medium values. Furthermore, among the 9 odd-numbered years, fire
176 activities in years 2003/2011/2013 show the highest three BC emission, which is also consistent
177 with results from the GFEDv4.1s dataset. Hence, the two independent fire emission inventories
178 agree on the interannual variation of fire activities.

179 Apart from cross-checking different fire emission inventories, we further validated the variability
180 of fire activities by investigating fire-induced changes in AOD (Fig. 1c). BC AOD from MERRA-
181 2 reanalysis and AOD of biomass burning aerosol type from CALIPSO were adopted to represent
182 fire activities. Basically, the interannual variation of fire-related AOD in both datasets agrees well
183 with the estimates from fire inventories, thus providing additional support for the quasi-biennial

184 variability of fire activities in the peak burning months over SMCA. Overall, the intercomparison
185 between multiple datasets indicates a consistent quasi-biennial variability in different fire
186 characteristics, including fire-consumed dry matter, fire-emitted aerosols as well as fire-related
187 changes in optical properties. Note that among the four datasets, the GFEDv4.1s inventory and
188 MERRA-2 reanalysis data provide data till the year of 2023, and the quasi-biennial variability in
189 the extended time series remains robust till 2023 (Fig. S1). To describe this quasi-biennial
190 variability for convenience, we hereafter refer to the odd-numbered (even-numbered) years that
191 have higher (lower) fire consumptions of dry matter than adjacent years as strong (weak) fire years.
192



194
 195
 196
 197
 198
 199
 200
 201
 202
 203
 204
 205

Figure 1. Interannual variations of different fire characteristics during the peak burning season (Apr-May) over Southern Mexico and Central America (SMCA). (a) Regional sum of the total dry matter consumed by fire activities based on the GFEDv4.1s emission data. (b) Distributions of the daily sum of fire-emitted black carbon (BC) over SMCA based on QFED emission data. Boxes denote the 25th and 75th percentiles. Bars outside the boxes denote the 10th and 90th percentiles. Bars within the boxes denote the medium values, and dots denote regional mean values (c) Regional mean aerosol optical depth (AOD) of smoke aerosols from CALIPSO product and BC AOD from MERRA-2 reanalysis. The odd-numbered years with strong fires are denoted by the grey bars.

206 **3.2 Dominant role of the biennial variability of precipitation**

207 Fire activity is strongly affected by factors including fire ignition, fuel load, and climate-weather
208 conditions (Flannigan et al., 2005; Archibald, 2016; Ichoku et al., 2016; Veira et al., 2016). Fire
209 ignition is affected by both natural lightning and human activities (Pechony and Shindell, 2009).
210 Since there is no policy to regulate fire activities with periodicity, it is unlikely that human impact
211 is the major driving force. Fuel availability may play a role in the interannual variation of fires.
212 After having examined the GPP (surrogate for fuel load) prior to the burning season, we found
213 little evidence regarding the role of fuel availability in contributing to the interannual variation of
214 fires (Fig. S3). Lower values of GPP are found in some strong fire years compared to their adjacent
215 years, e.g., the years 2003 and 2005. Correlations between regional GPP and fire-consumed dry
216 matter are even slightly negative. Moreover, correlations between the regional mean diffuse
217 radiative flux and fire-consumed dry matter are also statistically insignificant.

218 Close yet complex relationships between ambient conditions (e.g., humidity, temperature,
219 precipitation) and fire activities have been widely revealed in previous studies (Cary et al., 2006;
220 Gillett et al., 2004; Prasad et al., 2008). For example, warm temperatures could increase fire
221 activity by increasing evapotranspiration and also by lengthening fire duration, while both the
222 timing and amount of precipitation could regulate fire behavior. To identify the climatic factors
223 that might be responsible for the quasi-biennial variation of fire activities, we first examined the
224 relationships between fire-consumed dry matter and different meteorological variables (Table 1).
225 Temporal correlations of their regional mean values indicate that fire activities are enhanced with
226 warmer mean and maximum temperature ($R=0.47$ and 0.59), but are weakened with higher
227 precipitation ($R=-0.69$). Though wind speed could affect the spread of fire activities, the
228 insignificant correlation signifies a minor influence on the interannual scale (Fig. S3). Other
229 meteorological metrics such as vapor pressure deficit (VPD) and relative humidity (RH) are also
230 frequently used to help understand fire-meteorology interactions. Correlations in Table 1 indicate
231 that higher VPD facilitates fire activities while higher RH depresses fire activities. Here we found
232 that the interannual variations of regional mean VPD and RH are in fact highly correlated with
233 precipitation ($R = -0.8$ for VPD and $R=0.7$ for RH, respectively) and temperature ($R = 0.7$ for VPD
234 and $R = -0.5$ for RH, respectively) over the SMCA region.

235 Figure 2 shows the spatial distribution of correlations of fire-consumed dry matter with
236 precipitation and mean temperature during peak burning months. With respect to precipitation,

237 negative correlations cover almost the entire SMCA region and are statistically significant over
 238 major fire source areas from Yucatan extending southwestward to Chiapas. In contrast, positive
 239 correlations between fire-consumed dry matter and maximum temperature mainly appear over the
 240 northern part of SMCA (southern Mexico), albeit with less influence over Central America (e.g.,
 241 fire source areas in Guatemala). Hence, the interannual variability of precipitation affects the
 242 variation of fire activities on a wider spatial range. We next examined closely the time series of
 243 regional mean precipitation and temperature (Fig 3). Here regional mean values are calculated
 244 using data over land so that only climate conditions that could directly affect fire activities are
 245 considered. Two independent precipitation datasets show similar temporal evolution patterns. An
 246 obvious quasi-biennial variability is seen in regional mean precipitation. More suppressed
 247 precipitation (compared to adjacent years) corresponds well to the strong fire years (excluding the
 248 year 2016). Furthermore, spectral analysis confirms a statistically significant periodicity of
 249 approximately 2 years (0.042 cycles per month) for precipitation, suggesting the mediation of
 250 precipitation on the quasi-biennial feature of fire activities. Meanwhile, the quasi-biennial signal
 251 is less apparent in mean and maximum temperatures. For instance, temperatures in the strong fire
 252 years 2007 and 2009 are smaller in magnitude compared to adjacent weak fire years. Nevertheless,
 253 higher mean and maximum temperatures (compared to adjacent years) appear in 2003 and 2011,
 254 which combines with the suppressed precipitation, contributing to the abnormally high fire-
 255 consumed dry matter in the two years. As a result, while both temperature and precipitation are
 256 critical in shaping fire activities over the SMCA region, precipitation plays a more fundamental
 257 role in formulating the quasi-biennial variability of fires.

258

259 **Table 1.** Correlations between the regional sum of fire consumed dry matter based on the
 260 GFEDv4.1 data and regional mean values of different meteorological variables (including the
 261 monthly mean precipitation from IMERG dataset, mean temperature, maximum temperature from
 262 CRU dataset, and 10m wind speed from ERA5 reanalysis) averaged in the peak fire season (April-
 263 May).

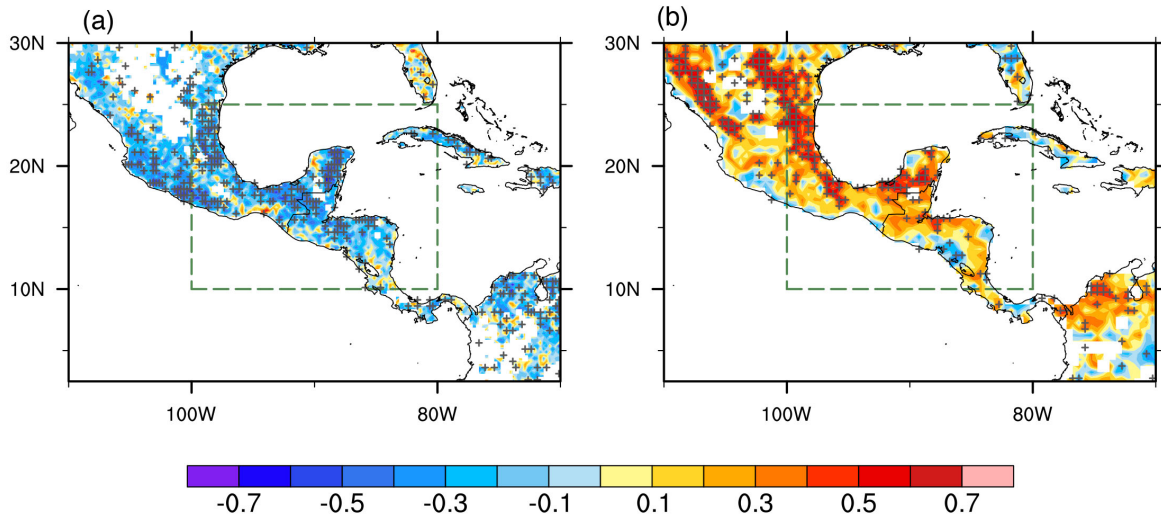
Correlation	Precipitation	Mean Temperature	Maximum Temperature	Relative humidity	Vapor pressure deficit	10m wind speed
Fire-consumed Dry matter	-0.69*	0.47*	0.59*	-0.63*	0.61*	0.29

264 * represents the correlations are statistically significant at the 90% confidence level based on the
265 student's T-test.

266

267

268



269

270

271

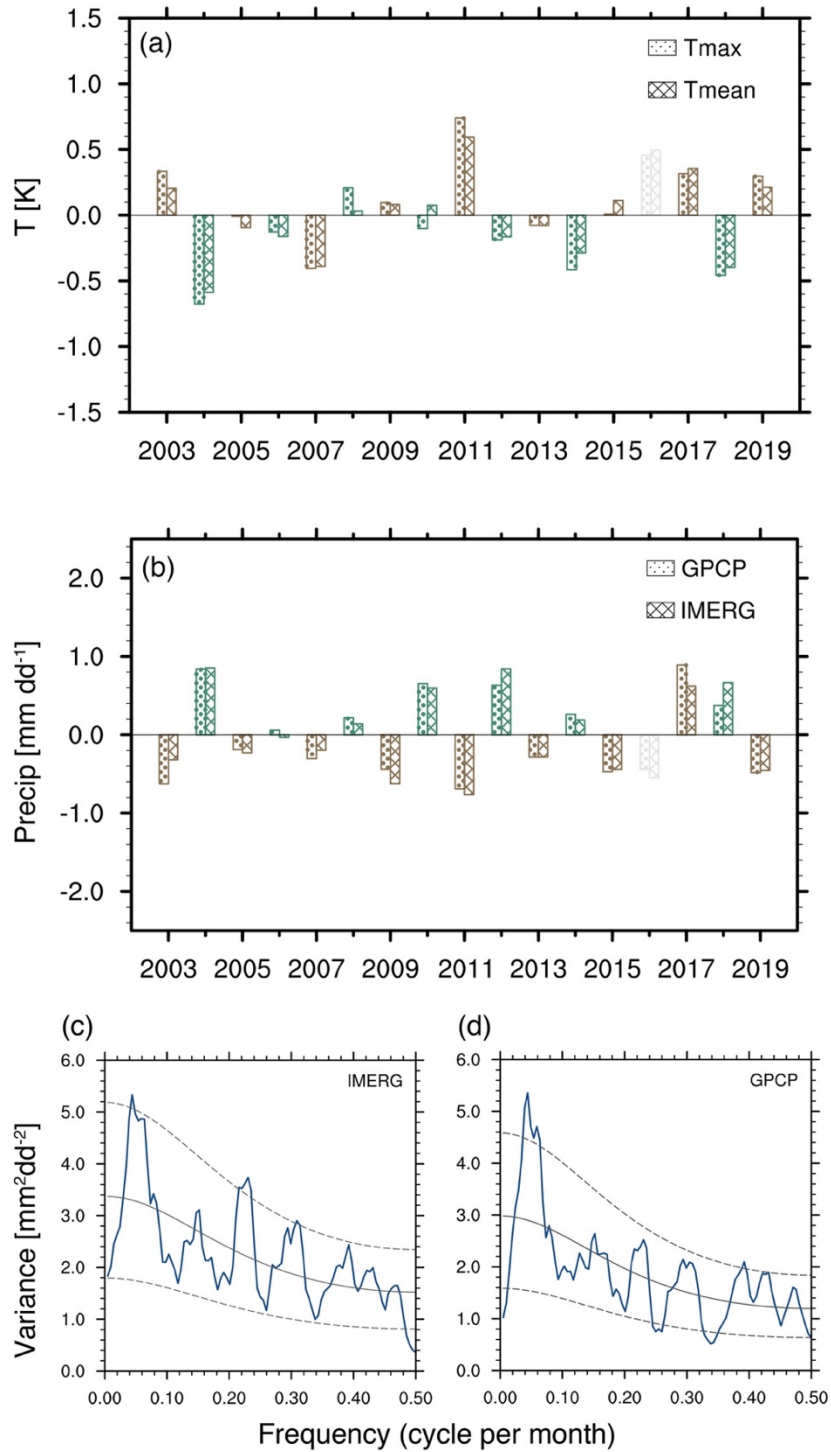
272

273

274

275

Figure 2. The influence of meteorological factors on fire activities over SMCA. Spatial distributions of grid-to-grid correlations between fire-consumed dry matter and (a) precipitation from IMERG and (b) maximum temperature from CRU during the peak fire season (Apr-May) over 2003-2019. Stippling indicates the correlations are statistically significant at the 90% confidence level based on the student's T-test. The green boxes denote the SMCA region.



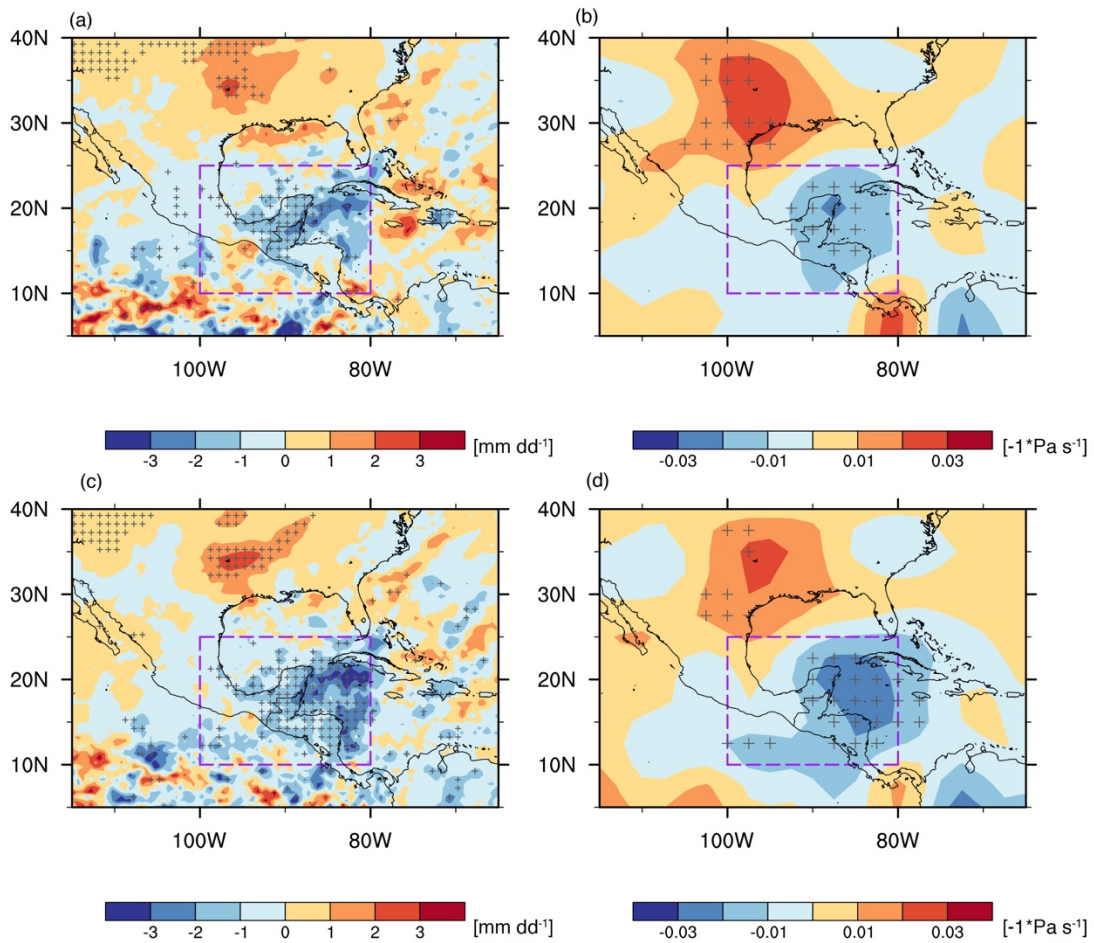
276
 277
 278
 279
 280
 281
 282
 283

Figure 3. Interannual variability of meteorological factors in peak fire season over SMCA. Time series of the Apr-May (a) mean/maximum temperature and (b) mean precipitation anomalies (with respect to the 2003-2019 climatology mean) averaged over SMCA (land only). (c) Spectral analysis of monthly mean precipitation averaged over SMCA during 2003-2019. The black solid line and dashed lines represent the red noise curve and the 10%, 90% confidence interval.

284 The leading role of precipitation on the interannually varying fire activities is evident in the
285 composite analysis, as shown by the contrast of reduced precipitation in strong fire years and
286 enhanced precipitation in weak fire years (Fig. 4a). The composite analysis further shows that the
287 anomalous precipitation is closely related to vertical motions, with stronger subsidence
288 corresponding to weaker precipitation (Fig. 4b). It is worth noting that to the northwest of the
289 SMCA region near the southeast US, composited precipitation and vertical velocity also differ
290 significantly between strong and weak fire years albeit of opposite signs. Consistent changing
291 features of precipitation and vertical velocity are also captured when regressing the two variables
292 on the regional mean precipitation over SMCA (Fig. 4c-d). The negative regression coefficients
293 indicate a stronger upward (downward) motion corresponding to higher (weaker) precipitation. In
294 sum, for a specific year, stronger subsidence and the subsequent suppression of precipitation tend
295 to amplify fire activity in that year, and vice versa for the year with weakened subsidence and less
296 suppression effect of precipitation. In this way, the quasi-biennial variability of precipitation leads
297 to the same interannual variability of fire activities.

298 Precipitation patterns over the SMCA region and the variability are associated with complex
299 physical forcing mechanisms, e.g. changes in sea surface temperature, low-level winds, the
300 strength and position of ITCZ et al., and all of these processes could be modulated by large-scale
301 modes of atmospheric and oceanic variability (Duran-Quesada et al., 2017; Perdigon-Morales et
302 al., 2019; Amador et al., 2006). Here we chose 10 typical teleconnection patterns, for example, the
303 El Niño-Southern Oscillation, (ENSO), based on previous studies and examined their relationships
304 with SMCA precipitation in the peak fire months. After calculating the correlations between Apr-
305 May mean precipitation and the index in varying months (both simultaneously and previous to the
306 fire season), we found that the precipitation in the fire season is mostly affected by the East
307 Pacific/North Pacific Oscillation (EP/NP) pattern in the previous two months (Feb-Mar).
308 Generally, the positive phase of EP/NP features negative height anomalies and an enhanced
309 cyclonic circulation over the eastern United States (Athanasiadis et al., 2010). Consequently, in
310 the following fire season, this causes anomalous upward and downward motions over the
311 southeastern US and the SMCA region respectively (Fig. S4), and enhances precipitation over the
312 southeastern US yet suppressing precipitation over the SMCA region (Fig. 5). Hence, the EP/NP
313 teleconnection results in an opposite responding pattern in precipitation and vertical velocity

314 between the eastern US and the SMCA region. This further explains the similar contrasting spatial
315 pattern that is found in the aforementioned composite and regression analysis.

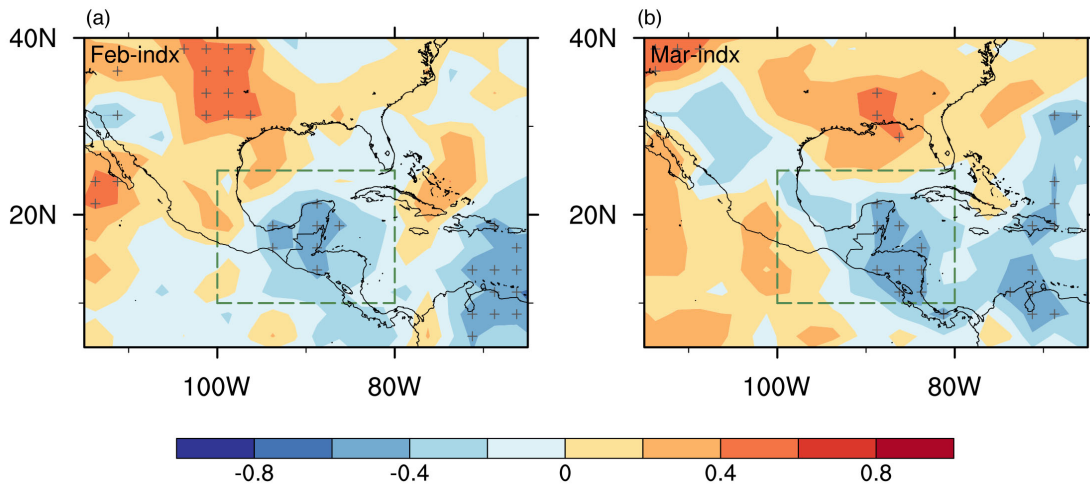


316
317

318 **Figure 4.** Varying characteristics of precipitation and circulations. Differences of composites of
319 (a) precipitation and (b) 500hPa vertical pressure velocity (reversed signs) between strong and
320 weak fire years. Stippling indicates the differences are statistically significant at the 90%
321 confidence level based on T-test. Regressions of Apr-May mean (c) precipitation and (d) 500hPa
322 vertical velocity on the regional mean precipitation over SMCA (reversed signs) during 2003-
323 2019. Stippling indicates regression coefficients are statistically significant at the 90% confidence
324 level based on the T-test.

325

326



327

328

329

330

331

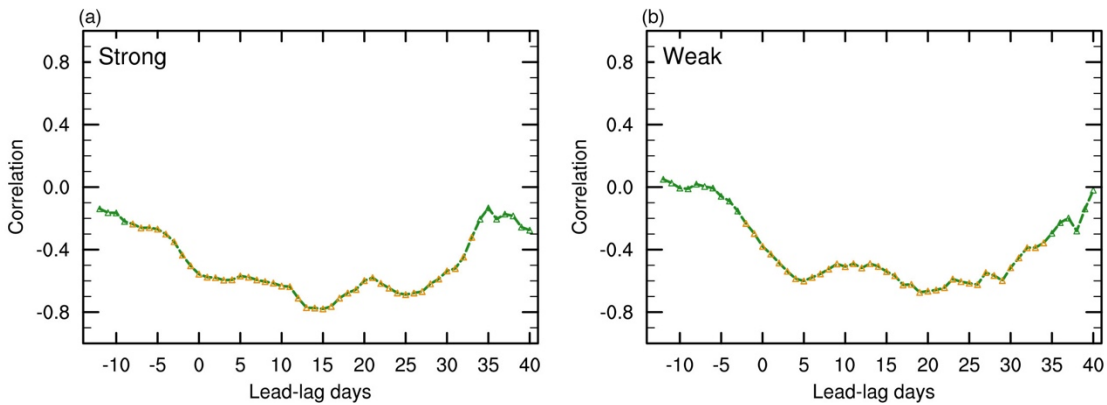
332

333

334

Figure 5. Influence of the EP/NP teleconnection pattern on precipitation in peak fire season. Spatial distributions of correlations of EP/NP index in (a) February and (b) March with the mean precipitation in the peak fire season (Apr-May) during 2003-2019. Stippling indicates the correlations are statistically significant based on the student's T-test.

335



336

337

338

339

340

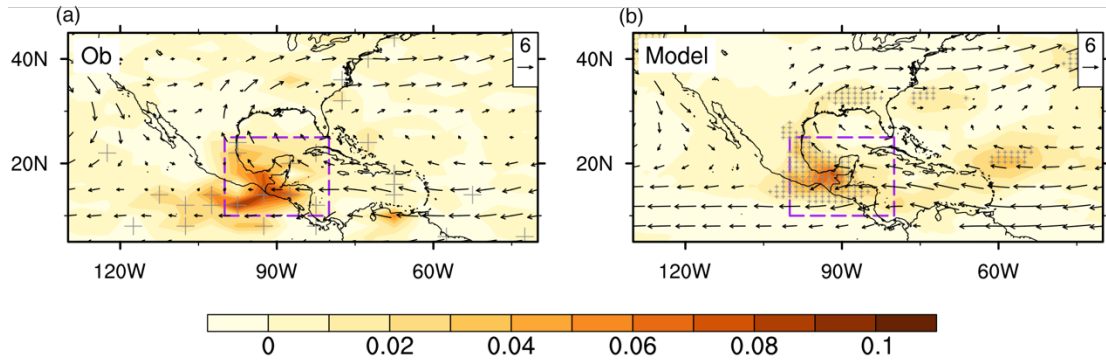
341

Figure 6. Different duration of fire-precipitation interaction. Lead-lag correlations between regional mean daily precipitation and fire emission composites in (a) strong fire years and (b) weak fire years over SMCA. Positive lead-lag days represent that precipitation leads while negative lead-lag days represent fire emissions leads. Correlations that are statistically significant at the 90% confidence level based on Student's t-test are marked with yellow triangles.

342 **3.3 Positive feedback between enhanced fire emissions and suppressed precipitation**

343 Previous studies have found that fire-emitted aerosols could interact with synoptic weather, which
344 in turn affects fire variability (Huang et al., 2023). In view of this, one concern is if fire and
345 precipitation interact on short timescales (i.e., within individual fire seasons) in our case over the
346 SMCA region, and if so, how this feedback modulates the quasi-biennial variability of
347 precipitation and fire activities. We first calculated lead-lag correlations between daily
348 precipitation and fire emissions to identify the short-term fire-precipitation interaction. As shown
349 in Fig. 6 lead-lag correlations between regional mean precipitation and fire emission are generally
350 similar whether fire activities in strong or weak fire years are considered. When precipitation leads,
351 precipitation negatively correlates with fire emission for more than 20 days, signifying a long-
352 lasting suppression effect of precipitation on fire activities. In other words, weakened precipitation
353 would enhance fire activities. Meanwhile, when fire leads, negative correlations indicate that
354 increased fire activities would further suppress precipitation at shorter timescales (3-5 days)
355 through rapid adjustments. In short, there is a two-way interaction between precipitation and fire
356 activities on short timescales with different duration, forming a positive feedback loop.

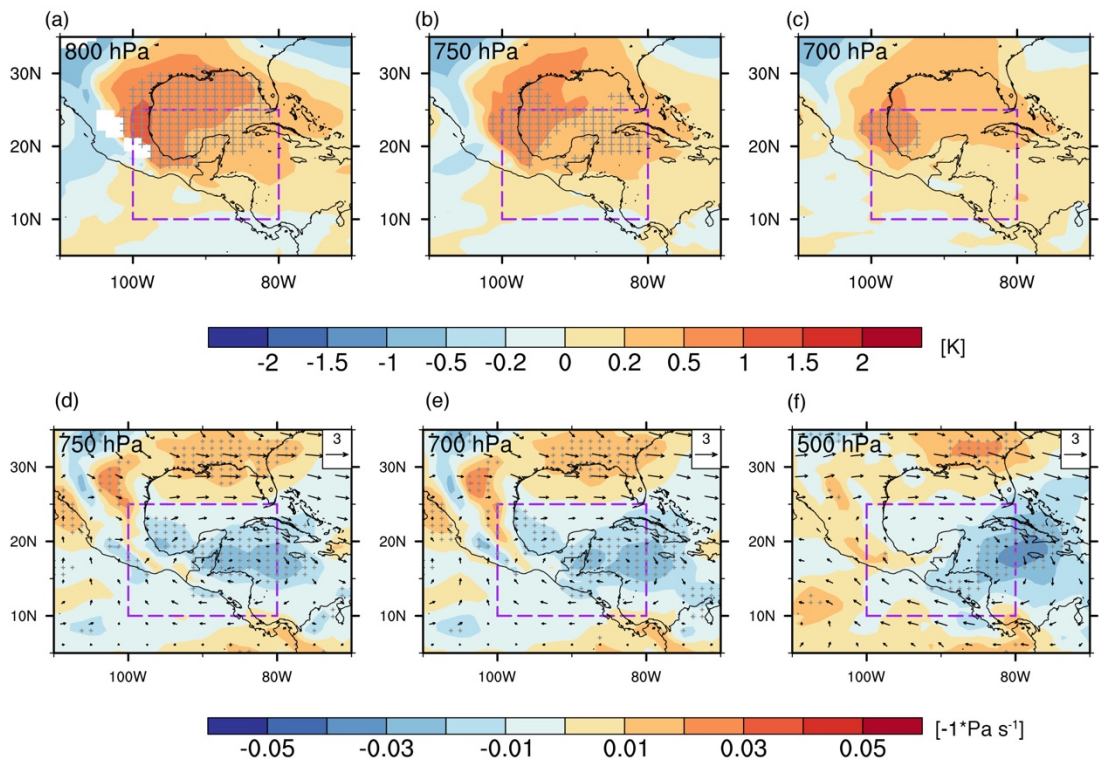
357 We also conducted sensitivity simulations to investigate the underlying processes involved in the
358 fire-precipitation feedback. Fig. 7 shows the simulated difference in AOD (referred to as fire AOD)
359 between Case_Strong and Case_Weak. Both the spatial pattern and magnitude agree well with the
360 difference in AOD between strong and weak fire years based on CALIPSO observations.
361 Compared to the spatial patterns of fire consumption in Fig. 7, we can clearly see two transport
362 pathways of fire-emitted aerosols due to the continental divide by the Central Mexican Plateau.
363 North of 15°N, fire-emitted aerosols are transported northward by the subtropical high, among
364 which large amounts accumulate over the downstream Gulf of Mexico due to the block of the high
365 terrain, and the rest is further transported northward reaching the southeastern US; South of 15°N,
366 prevailing easterlies transport fire-emitted aerosols directly westward, far away to the eastern
367 Pacific.



368
369

370 **Figure 7.** Evaluation of model simulated fire-induced AOD. (a) Spatial distributions of differences
371 in biomass burning AOD between strong and weak fire years from CALIPSO satellite data. (b)
372 Differences in simulated AOD between Case_Strong and Case_Weak. Mean 850hPa wind vectors
373 from (a) NCEP reanalysis data averaged in all years and (b) model simulations averaged between
374 both cases are overlaid respectively. Stippling indicates the differences in AOD are statistically
375 significant based on T-test.

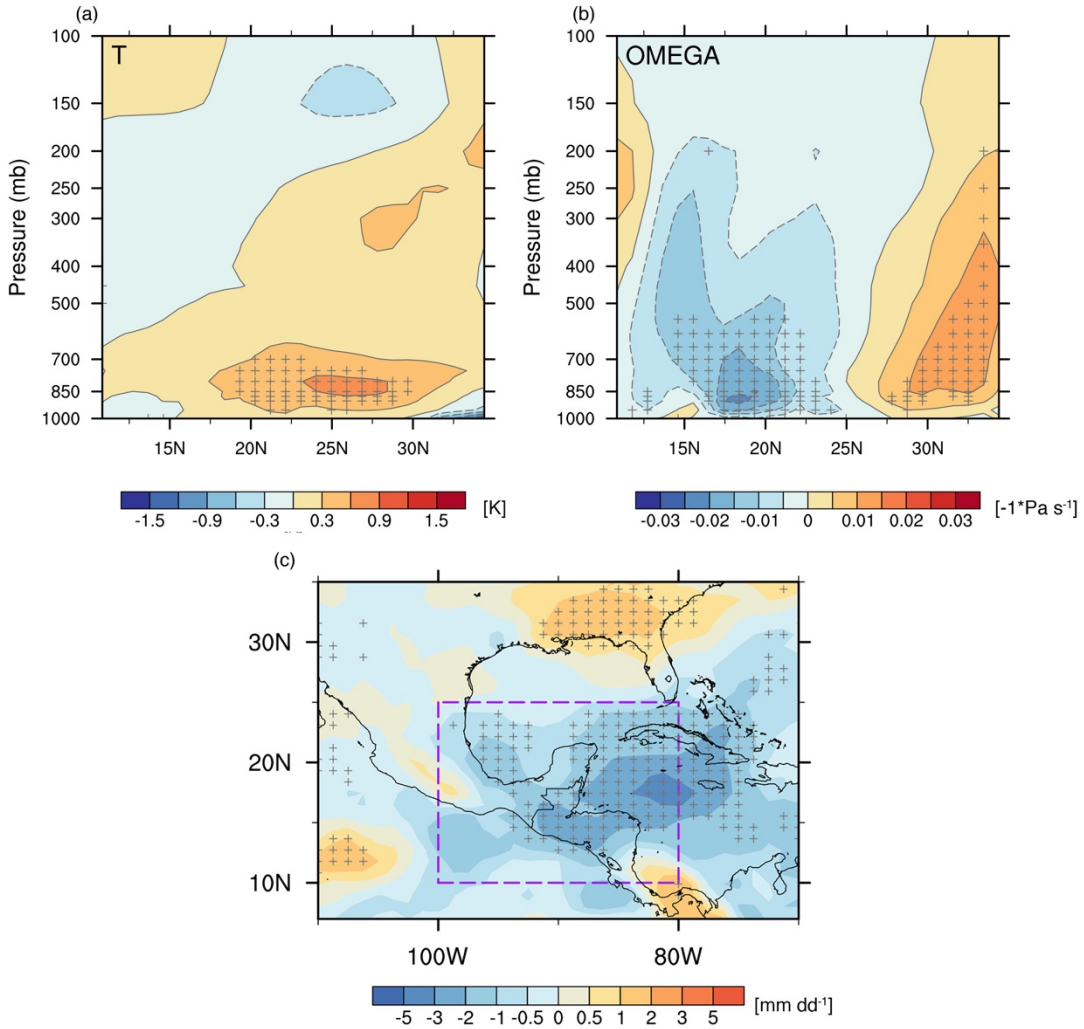
376



377
378

379 **Figure 8.** Changes in meteorological variables induced by fire-emitted aerosols. Differences in (a-
380 c) atmospheric temperature and (d-f) vertical pressure velocity (reversed signs and shaded colors)
381 at different vertical levels between Case_Strong and Case_Weak. Changes in horizontal winds
382 between the two cases are overlaid in (d-f). Stippling indicates the differences are statistically
383 significant at the 90% confidence level based on T-test.

384 Considering the northward pathway, with the stack of light-absorbing BC aerosols, air temperature
385 warms up by approximately 1-2K, and this warming extends from 800hPa to 700hPa where BC
386 aerosols suspend (Fig. 8a-c). Vertical slices of the temperature anomalies indicate significant
387 warming to the north (downstream) of the fire source regions (Fig. 9a). In response to this warming,
388 the air above the fire aerosol layers rises up (Fig. 8d-f). The anomalous ascending motion covers
389 from the Gulf of Mexico to the southeastern US, with the maximum center located near the Gulf
390 of Mexico. This abnormal ascending motion, on one hand, enhances precipitation downstream of
391 the fire source regions, and on the other hand forces a compensating anomalous descending motion
392 over the SMCA region and suppresses the precipitation over the fire source regions (Fig. 9b-c).
393 This simulated opposite change in precipitation resembles the spatial pattern of the composited
394 precipitation difference between strong and weak fire years (Fig. 4a), suggesting that fire-
395 precipitation interaction reinforces the contrast of precipitation between strong and weak fire years.
396 Therefore, the model simulations confirm a positive fire-precipitation feedback loop on the short
397 timescale within the fire season. Though variations of RH could influence fire activities on
398 interannual scales, the short-term feedback of fire aerosols on near surface RH are much weaker
399 compared to precipitation (Fig. S5).



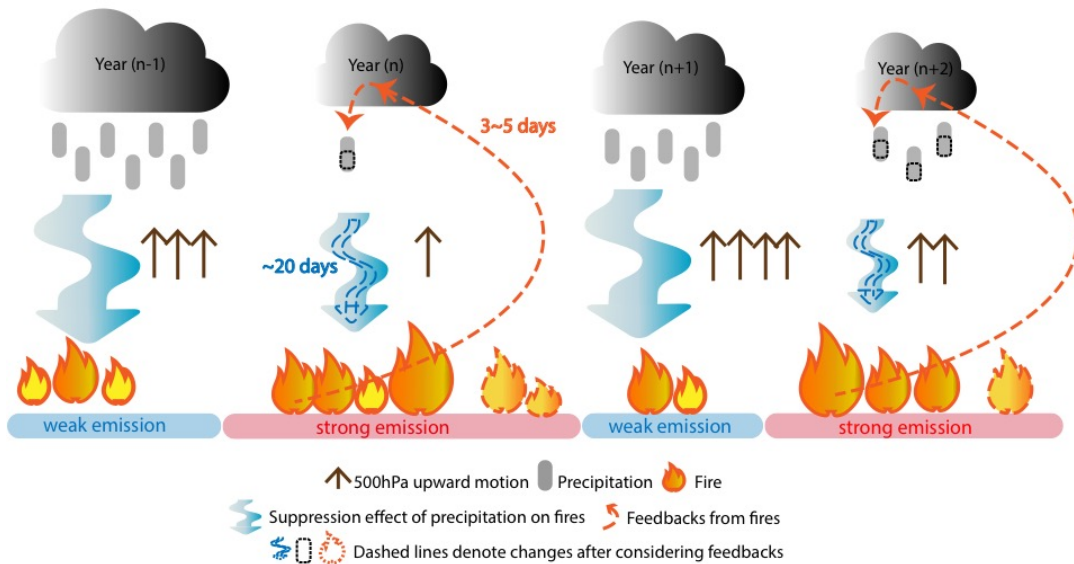
400
 401
 402 **Figure 9.** Vertical slices of differences in (a) atmospheric temperature and (b) pressure velocity
 403 averaged along $[80^\circ - 100^\circ \text{W}]$ between Case_Strong and Case_Weak. (c) Differences in
 404 precipitation between Case_Strong and Case_Weak. Stippling indicates the differences are
 405 statistically significant based on T-test.

406
 407 As illustrated in Fig. 10, originally on the interannual scale, fire activities over the SMCA region
 408 exhibit a significant quasi-biennial variability that is predominantly determined by the quasi-
 409 biennial variation of precipitation. On this basis, there is an additional two-way interaction between
 410 fire and precipitation on short timescales. Typically, precipitation suppresses fire activities with a
 411 time lag of more than 20 days, while fire-emitted aerosols suppress precipitation by modifying
 412 circulations with a timescale of 3-5 days. That is to say, for a year with abnormally weak
 413 precipitation, fire activities would get amplified, which in turn further weakens precipitation. In

414 this way, the short-term positive feedback loop ultimately enhances the quasi-biennial variability
415 of precipitation and fire activities over the SMCA region.

416

417



418

419 **Figure 10.** A schematic diagram illustrating how multi-scale fire-precipitation interactions shape
420 the quasi-biennial variability of fires over SMCA. On the interannual scale, the quasi-biennially
421 varying precipitation triggers a similar quasi-biennial variability of fire activities via its
422 suppression effect. Compared to adjacent years, a weaker precipitation year will facilitate stronger
423 fires. On short timescales within each fire season, there is a positive feedback loop between fire
424 and precipitation (denoted by dashed lines). The suppression effect of precipitation lasts long for
425 approximately 20 days, while fires affect precipitation through a rapid adjustment of 3-5 days. In
426 the weaker precipitation year, stronger fire activities emit more aerosols, which by mediating
427 temperature and circulations, ultimately suppress precipitation over the fire source region. Such
428 short-term interactions between precipitation and fire amplify the magnitude of anomalous fire and
429 precipitation in individual years and enhance the quasi-biennial variability of both precipitation
430 and fire.

431 **4 Conclusion and Discussion**

432 Fires play an important role in the Earth system, and the complex interaction between fire activities
433 and ambient conditions poses a great challenge to fire prediction and management. This study
434 identifies a distinct quasi-biennial variability of fire activities over the SMCA region during 2003-
435 2019 on the basis of different fire metrics. Both the bottom-up (GFEDv4.1s) and top-down(QFED)
436 emission inventories show relatively higher fire consumption (or emission) in the odd-numbered
437 years than the adjacent even-numbered years with the only exception of the year 2016. Moreover,
438 fire-induced changes in AOD also reveal consistent quasi-biennial variation.

439 By examining the relationships between fire consumption and different meteorological variables,
440 our analysis indicates that the quasi-biennial signal is dominated by the quasi-biennially varying
441 precipitation, while the influence of temperature is mostly reflected in a few extremely strong fire
442 years. Typically, strong fire years correspond to suppressed upward motions and weakened
443 precipitation. The quasi-biennial variability of precipitation is seen in the time series of the regional
444 mean precipitation over SMCA and the spectral analysis, and is closely related to the EP-NP
445 teleconnection pattern in the two months previous to the fire season. The positive phase of the EP-
446 NP pattern implies enhanced precipitation over the southeastern US (downstream of the SMCA),
447 albeit reduced precipitation over the SMCA region.

448 On the other hand, we further found that positive feedback exists between fire-emitted aerosols
449 and precipitation on short timescales and acts to amplify the quasi-biennial oscillations in both fire
450 and precipitation over the SMCA region. Lead-lag correlations between daily fire emission and
451 precipitation suggest that the two-way interactions occur with different duration. The suppression
452 effect of precipitation lasts for approximately 20 days, while fire-emitted aerosols weaken
453 precipitation through rapid adjustments of 3-5 days. Furthermore, model simulations reveal that
454 compared to weak fire years, more fire-emitted aerosols are transported downstream and
455 accumulate near the Gulf of Mexico in strong fire years. These suspended light-absorbing BC
456 aerosols warm the low-level atmosphere by 1-2K and induce anomalous ascending motion aloft
457 700hPa. A compensating descending motion is subsequently forced over the SMCA region, which
458 ultimately suppresses the precipitation over the fire source region and hence forms a positive
459 feedback loop.

460 These findings provide useful information relevant to the fire control and mitigation of air quality
461 over the SMCA region. Given that fire activities over the SMCA represent a typical tropical fire
462 regime, our work may also provide new insight into some fundamental features of fires in the Earth
463 System. The mechanism may also operate elsewhere useful on the planet. While precipitation is
464 demonstrated to play the primary role in determining the periodicity of fire activities over the
465 SMCA region, the fundamental cause of the quasi-biennial variability of precipitation is unknown.
466 Currently, we have only shown that the EP-NP teleconnection, among all selected indexes, exerts
467 the most influence on the interannual variability of precipitation. Other teleconnection patterns,
468 e.g., ENSO, despite their insignificant correlations with SMCA precipitation, may affect the
469 circulation and precipitation over the southeastern US or over the neighboring Intra-American Sea
470 (Anthony Chen and Taylor, 2002), and hence might more or less affect the precipitation over the
471 SMCA region. Moreover, though we demonstrated positive feedback between fire-emitted
472 aerosols and precipitation exists on short timescales, to what extent this feedback contributes to
473 the quasi-biennial variability of fire activities remains unquantified due to the absence of coupled
474 fire-climate interactions in current model simulations. Future efforts to quantify how different
475 factors and feedback work together to shape the quasi-biennial variability of precipitation and fire
476 activities using interactive fire-climate models would further benefit the prediction and
477 management of fire activities over the SMCA region.

478 **Data availability**

479 The GFED v4.1s fire emission data is available at <http://www.globalfiredata.org/data.html>.
480 The CRU TS v.4.06 can be found at <https://crudata.uea.ac.uk/cru/data/hrg/>. The QFEDv2.5 data
481 can be found at <http://ftp.as.harvard.edu/gcgrid/data/ExtData/HEMCO/QFED/v2018-07/>. The
482 MODIS GPP data is available from
483 <https://lpdaac.usgs.gov/products/mod17a2hv061/>The MERRA-2 reanalysis data can be found at
484 https://gmao.gsfc.nasa.gov/reanalysis/MERRA-2/data_access/. The IMERG precipitation dataset
485 can be obtained from <https://gpm.nasa.gov/data/imerg>. The GPCP dataset can be obtained from
486 <https://www.ncei.noaa.gov/products/climate-data-records/precipitation-gpcp-daily>.
487 Teleconnection indices can be found at <https://psl.noaa.gov/data/climateindices/list/>. The NCEP-
488 NCAR reanalysis is obtained from
489 <https://www.esrl.noaa.gov/psd/data/gridded/data.ncep.reanalysis2.html>.
490 The CALIPSO product is available at
491 https://asdc.larc.nasa.gov/project/CALIPSO/CAL_LID_L3_Tropospheric_APro_AllSky-Standard-V4-20_V4-20.

493

494 **Author contribution**

495 Y.L. and Y. Q. conceived of the presented idea. Y. Q., Y. W. and Y. L. developed the theory. Y.
496 L. performed the computations and verified the methods. Y. Q., Y. L. and K. Z wrote the first draft
497 of the manuscript. All authors contributed to the interpretation of the results and writing/revision
498 of the final manuscript.

499

500 **Competing interests**

501 Yun Qian and Hailong Wang are members of the editorial board of Atmospheric Chemistry and
502 Physics. The authors have no other competing interests to declare.

503

504 **Acknowledgments**

505 We benefited from discussing some aspects of this work with John M Wallace and Dae-Hyun Kim.
506 Yawen Liu is supported by the National Natural Science Foundation of China (No. 42325506).
507 This research is also supported by the US Department of Energy Office of Science Biological and
508 Environmental Research as part of the Regional and Global Model Analysis and Multi-Sector
509 Dynamics programme areas. The Pacific Northwest National Laboratory is operated for DOE by
510 Battelle Memorial Institute under contract DE-AC05-76RL01830. We are grateful to the High-
511 Performance Computing (HPC) and the Massive Data Center (MDC) at Nanjing University for
512 the numerical calculations.

513

514

515

516

517 **References**

- 518 Abram, N. J., Henley, B. J., Sen Gupta, A., Lippmann, T. J. R., Clarke, H., Dowdy, A. J., Sharples, J. J., Nolan, R. H.,
519 Zhang, T. R., Wooster, M. J., Wurtzel, J. B., Meissner, K. J., Pitman, A. J., Ukkola, A. M., Murphy, B. P., Tapper, N.
520 J., and Boer, M. M.: Connections of climate change and variability to large and extreme forest fires in southeast
521 Australia, *Commun Earth Environ*, 2, ARTN 810.1038/s43247-020-00065-8, 2021.
- 522 Adler, R. F., Sapiano, M. R. P., Huffman, G. J., Wang, J. J., Gu, G. J., Bolvin, D., Chiu, L., Schneider, U., Becker,
523 A., Nelkin, E., Xie, P. P., Ferraro, R., and Shin, D. B.: The Global Precipitation Climatology Project (GPCP) Monthly
524 Analysis (New Version 2.3) and a Review of 2017 Global Precipitation, *Atmosphere*, 9, ARTN
525 13810.3390/atmos9040138, 2018.
- 526 Adler, R. W., Jian-Jian; Sapiano, Mathew; Huffman, George; Bolvin, David; Nelkin, Eric; and NOAA CDR Program:
527 Global Precipitation Climatology Project (GPCP) Climate Data Record (CDR), Version 1.3 (Daily), NOAA National
528 Centers for Environmental Information. doi:10.7289/V5RX998Z, 2017.
- 529 Aguilera, R., Corringham, T., Gershunov, A., and Benmarhnia, T.: Wildfire smoke impacts respiratory health more
530 than fine particles from other sources: observational evidence from Southern California, *Nature Communications*, 12,
531 ARTN 149310.1038/s41467-021-21708-0, 2021.
- 532 Amador, J. A., Alfaro, E. J., Lizano, O. G., and Magana, V. O.: Atmospheric forcing of the eastern tropical Pacific: A
533 review, *Prog Oceanogr*, 69, 101-142, 10.1016/j.pocean.2006.03.007, 2006.
- 534 Anthony Chen, A. and Taylor, M. A.: Investigating the link between early season Caribbean rainfall and the El Niño
535 + 1 year, *International Journal of Climatology*, 22, 87-106, 10.1002/joc.711, 2002.
- 536 Archibald, S.: Managing the human component of fire regimes: lessons from Africa, *Philosophical Transactions of
537 the Royal Society B: Biological Sciences*, 371, 20150346, 2016.
- 538 Athanasiadis, P. J., Wallace, J. M., and Wettstein, J. J.: Patterns of Wintertime Jet Stream Variability and Their
539 Relation to the Storm Tracks, *J Atmos Sci*, 67, 1361-1381, 10.1175/2009jas3270.1, 2010.
- 540 Bond, T. C., Doherty, S. J., Fahey, D., Forster, P., Berntsen, T., DeAngelo, B., Flanner, M., Ghan, S., Kärcher, B.,
541 and Koch, D.: Bounding the role of black carbon in the climate system: A scientific assessment, *Journal of Geophysical
542 Research: Atmospheres*, 118, 5380-5552, 2013.
- 543 Bowman, D. M., Balch, J. K., Artaxo, P., Bond, W. J., Carlson, J. M., Cochrane, M. A., D'Antonio, C. M., DeFries,
544 R. S., Doyle, J. C., and Harrison, S. P.: Fire in the Earth system, *science*, 324, 481-484, 2009.
- 545 Bowman, D. M. J. S., Williamson, G. J., Abatzoglou, J. T., Kolden, C. A., Cochrane, M. A., and Smith, A. M. S.:
546 Human exposure and sensitivity to globally extreme wildfire events, *Nat Ecol Evol*, 1, ARTN 005810.1038/s41559-
547 016-0058, 2017.
- 548 Cary, G. J., Keane, R. E., Gardner, R. H., Lavorel, S., Flannigan, M. D., Davies, I. D., Li, C., Lenihan, J. M., Rupp,
549 T. S., and Mouillot, F.: Comparison of the sensitivity of landscape-fire-succession models to variation in terrain, fuel
550 pattern, climate and weather, *Landscape ecology*, 21, 121-137, 2006.
- 551 Chiodi, A. M., Potter, B. E., and Larkin, N. K.: Multi-Decadal Change in Western US Nighttime Vapor Pressure
552 Deficit, *Geophysical Research Letters*, 48, ARTN e2021GL092830.1029/2021GL092830, 2021.
- 553 Crouse, J., DeCarlo, P., Blake, D. R., Emmons, L., Campos, T., Apel, E., Clarke, A., Weinheimer, A., McCabe, D.,
554 and Yokelson, R. J.: Biomass burning and urban air pollution over the Central Mexican Plateau, *Atmospheric
555 Chemistry and Physics*, 9, 4929-4944, 2009.
- 556 Crutzen, P. J. and Andreae, M. O.: Biomass Burning in the Tropics - Impact on Atmospheric Chemistry and
557 Biogeochemical Cycles, *Science*, 250, 1669-1678, DOI 10.1126/science.250.4988.1669, 1990.
- 558 Danabasoglu, G., Lamarque, J. F., Bacmeister, J., Bailey, D. A., DuVivier, A. K., Edwards, J., Emmons, L. K., Fasullo,
559 J., Garcia, R., Gettelman, A., Hannay, C., Holland, M. M., Large, W. G., Lauritzen, P. H., Lawrence, D. M., Lenaerts,
560 J. T. M., Lindsay, K., Lipscomb, W. H., Mills, M. J., Neale, R., Oleson, K. W., Otto-Bliesner, B., Phillips, A. S.,
561 Sacks, W., Tilmes, S., van Kampenhou, L., Verstein, M., Bertini, A., Dennis, J., Deser, C., Fischer, C., Fox-
562 Kemper, B., Kay, J. E., Kinnison, D., Kushner, P. J., Larson, V. E., Long, M. C., Mickelson, S., Moore, J. K.,
563 Nienhouse, E., Polvani, L., Rasch, P. J., and Strand, W. G.: The Community Earth System Model Version 2 (CESM2),
564 *J Adv Model Earth Sy*, 12, ARTN e2019MS00191610.1029/2019MS001916, 2020.
- 565 Ding, K., Huang, X., Ding, A. J., Wang, M. H., Su, H., Kerminen, V. M., Petaja, T., Tan, Z. M., Wang, Z. L., Zhou,
566 D. R., Sun, J. N., Liao, H., Wang, H. J., Carslaw, K., Wood, R., Zuidema, P., Rosenfeld, D., Kulmala, M., Fu, C. B.,
567 Poschl, U., Cheng, Y. F., and Andreae, M. O.: Aerosol-boundary-layer-monsoon interactions amplify semi-direct

568 effect of biomass smoke on low cloud formation in Southeast Asia, *Nature Communications*, 12, ARTN
569 641610.1038/s41467-021-26728-4, 2021.

570 Duran-Quesada, A. M., Gimeno, L., and Amador, J.: Role of moisture transport for Central American precipitation,
571 *Earth Syst Dynam*, 8, 147-161, 10.5194/esd-8-147-2017, 2017.

572 Fang, K. Y., Yao, Q. C., Guo, Z. T., Zheng, B., Du, J. H., Qi, F. Z., Yan, P., Li, J., Ou, T. H., Liu, J., He, M. S., and
573 Trouet, V.: ENSO modulates wildfire activity in China, *Nature Communications*, 12, ARTN 176410.1038/s41467-
574 021-21988-6, 2021.

575 Fasullo, J. T., Rosenbloom, N., and Buchholz, R.: A multiyear tropical Pacific cooling response to recent Australian
576 wildfires in CESM2, *Science Advances*, 9, eadg1213, 2023.

577 Flannigan, M. D., Krawchuk, M. A., de Groot, W. J., Wotton, B. M., and Gowman, L. M.: Implications of changing
578 climate for global wildland fire, *International journal of wildland fire*, 18, 483-507, 2009.

579 Flannigan, M. D., Logan, K. A., Amiro, B. D., Skinner, W. R., and Stocks, B.: Future area burned in Canada, *Climatic
580 change*, 72, 1-16, 2005.

581 Gelaro, R., McCarty, W., Suarez, M. J., Todling, R., Molod, A., Takacs, L., Randles, C. A., Darmenov, A., Bosilovich,
582 M. G., Reichle, R., Wargan, K., Coy, L., Cullather, R., Draper, C., Akella, S., Buchard, V., Conaty, A., da Silva, A.
583 M., Gu, W., Kim, G. K., Koster, R., Lucchesi, R., Merkova, D., Nielsen, J. E., Partyka, G., Pawson, S., Putman, W.,
584 Rienecker, M., Schubert, S. D., Sienkiewicz, M., and Zhao, B.: The Modern-Era Retrospective Analysis for Research
585 and Applications, Version 2 (MERRA-2), *J Climate*, 30, 5419-5454, 10.1175/Jcli-D-16-0758.1, 2017.

586 Giglio, L., Randerson, J. T., and Werf, G. R.: Analysis of daily, monthly, and annual burned area using the fourth -
587 generation global fire emissions database (GFED4), *Journal of Geophysical Research: Biogeosciences*, 118, 317-328,
588 2013.

589 Gillett, N., Weaver, A., Zwiers, F., and Flannigan, M.: Detecting the effect of climate change on Canadian forest fires,
590 *Geophysical Research Letters*, 31, 2004.

591 Harris, I., Jones, P., Osborn, T., and Lister, D.: Updated high - resolution grids of monthly climatic observations -
592 the CRU TS3. 10 Dataset, *International Journal of Climatology*, 34, 623-642, 2014.

593 Hersbach, H., Bell, B., Berrisford, P., Hirahara, S., Horanyi, A., Munoz-Sabater, J., Nicolas, J., Peubey, C., Radu, R.,
594 Schepers, D., Simmons, A., Soci, C., Abdalla, S., Abellan, X., Balsamo, G., Bechtold, P., Biavati, G., Bidlot, J.,
595 Bonavita, M., De Chiara, G., Dahlgren, P., Dee, D., Diamantakis, M., Dragani, R., Flemming, J., Forbes, R., Fuentes,
596 M., Geer, A., Haimberger, L., Healy, S., Hogan, R. J., Holm, E., Janiskova, M., Keeley, S., Laloyaux, P., Lopez, P.,
597 Lupu, C., Radnoti, G., de Rosnay, P., Rozum, I., Vamborg, F., Villaume, S., and Thepaut, J. N.: The ERA5 global
598 reanalysis, *Quarterly Journal of the Royal Meteorological Society*, 146, 1999-2049, 10.1002/qj.3803, 2020.

599 Huang, X., Ding, K., Liu, J. Y., Wang, Z. L., Tang, R., Xue, L., Wang, H. K., Zhang, Q., Tan, Z. M., Fu, C. B., Davis,
600 S. J., Andreae, M. O., and Ding, A. J.: Smoke-weather interaction affects extreme wildfires in diverse coastal regions,
601 *Science*, 379, 457-461, 10.1126/science.add9843, 2023.

602 Huffman, G. J., Bolvin, D. T., Nelkin, E. J., and Tan, J.: Integrated Multi-satellitE Retrievals for GPM (IMERG)
603 technical documentation, Nasa/Gsfc Code, 612, 2019, 2015.

604 Huffman, G. J., Bolvin, D. T., Braithwaite, D., Hsu, K.-L., Joyce, R. J., Kidd, C., Nelkin, E. J., Sorooshian, S., Stocker,
605 E. F., and Tan, J.: Integrated multi-satellite retrievals for the global precipitation measurement (GPM) mission
606 (IMERG), *Satellite Precipitation Measurement: Volume 1*, 343-353, 2020.

607 Ichoku, C., Ellison, L. T., Willmot, K. E., Matsui, T., Dezfuli, A. K., Gatebe, C. K., Wang, J., Wilcox, E. M., Lee, J.,
608 and Adegoke, J.: Biomass burning, land-cover change, and the hydrological cycle in Northern sub-Saharan Africa,
609 *Environmental Research Letters*, 11, 095005, 2016.

610 Jiang, Y. Q., Yang, X. Q., Liu, X. H., Qian, Y., Zhang, K., Wang, M. H., Li, F., Wang, Y., and Lu, Z.: Impacts of
611 Wildfire Aerosols on Global Energy Budget and Climate: The Role of Climate Feedbacks, *J Climate*, 33, 3351-3366,
612 10.1175/Jcli-D-19-0572.1, 2020.

613 Jolly, W. M., Cochrane, M. A., Freeborn, P. H., Holden, Z. A., Brown, T. J., Williamson, G. J., and Bowman, D. M.
614 J. S.: Climate-induced variations in global wildfire danger from 1979 to 2013, *Nature Communications*, 6, ARTN
615 753710.1038/ncomms8537, 2015.

616 Kanamitsu, M., Ebisuzaki, W., Woollen, J., Yang, S.-K., Hnilo, J., Fiorino, M., and Potter, G.: NCEP-DOE AMIP-II
617 Reanalysis (R-2), *B Am Meteorol Soc*, 83, 1631-1644, 2002.

618 Knorr, W., Dentener, F., Lamarque, J. F., Jiang, L. W., and Arneeth, A.: Wildfire air pollution hazard during the 21st
619 century, *Atmos Chem Phys*, 17, 9223-9236, 10.5194/acp-17-9223-2017, 2017.

620 Koster, R. D., Darmenov, A. S., and da Silva, A. M.: The quick fire emissions dataset (QFED): Documentation of
621 versions 2.1, 2.2 and 2.4, 2015.

622 Kreidenweis, S. M., Remer, L. A., Brientjes, R., and Dubovik, O.: Smoke aerosol from biomass burning in Mexico:
623 Hygroscopic smoke optical model, *Journal of Geophysical Research: Atmospheres*, 106, 4831-4844, 2001.

624 Lee, Y. S., Collins, D. R., Li, R., Bowman, K. P., and Feingold, G.: Expected impact of an aged biomass burning
625 aerosol on cloud condensation nuclei and cloud droplet concentrations, *Journal of Geophysical Research:*
626 *Atmospheres*, 111, 2006.

627 Liu, Y. W., Zhang, K., Qian, Y., Wang, Y. H., Zou, Y. F., Song, Y. J., Wan, H., Liu, X. H., and Yang, X. Q.:
628 Investigation of short-term effective radiative forcing of fire aerosols over North America using nudged hindcast
629 ensembles, *Atmos Chem Phys*, 18, 31-47, 10.5194/acp-18-31-2018, 2018.

630 Lu, Z., Liu, X., Zhang, Z., Zhao, C., Meyer, K., Rajapakshe, C., Wu, C., Yang, Z., and Penner, J. E.: Biomass smoke
631 from southern Africa can significantly enhance the brightness of stratocumulus over the southeastern Atlantic Ocean,
632 *Proceedings of the National Academy of Science*, 201713703, 2018.

633 Magi, B., Rabin, S., Shevliakova, E., and Pacala, S.: Separating agricultural and non-agricultural fire seasonality at
634 regional scales, *Biogeosciences*, 9, 3003, 2012.

635 Marlon, J. R., Bartlein, P. J., Carcaillet, C., Gavin, D. G., Harrison, S. P., Higuera, P. E., Joos, F., Power, M., and
636 Prentice, I.: Climate and human influences on global biomass burning over the past two millennia, *Nature Geoscience*,
637 1, 697-702, 2008.

638 Mouillot, F. and Field, C. B.: Fire history and the global carbon budget: a 1×1 fire history reconstruction for the 20th
639 century, *Global Change Biology*, 11, 398-420, 2005.

640 Page, S. E., Siegert, F., Rieley, J. O., Boehm, H. D. V., Jaya, A., and Limin, S.: The amount of carbon released from
641 peat and forest fires in Indonesia during 1997, *Nature*, 420, 61-65, 10.1038/nature01131, 2002.

642 Pechony, O. and Shindell, D.: Fire parameterization on a global scale, *Journal of Geophysical Research: Atmospheres*,
643 114, 2009.

644 Perdigon-Morales, J., Romero-Centeno, R., Barrett, B. S., and Ordonez, P.: Intraseasonal Variability of Summer
645 Precipitation in Mexico: MJO Influence on the Midsummer Drought, *J Climate*, 32, 2313-2327, 10.1175/Jcli-D-18-
646 0425.1, 2019.

647 Power, M. J., Marlon, J., Ortiz, N., Bartlein, P. J., Harrison, S. P., Mayle, F. E., Ballouche, A., Bradshaw, R. H.,
648 Carcaillet, C., and Cordova, C.: Changes in fire regimes since the Last Glacial Maximum: an assessment based on a
649 global synthesis and analysis of charcoal data, *Climate dynamics*, 30, 887-907, 2008.

650 Prasad, V. K., Badarinath, K., and Eaturu, A.: Biophysical and anthropogenic controls of forest fires in the Deccan
651 Plateau, India, *Journal of Environmental Management*, 86, 1-13, 2008.

652 Randerson, J., Chen, Y., Werf, G., Rogers, B., and Morton, D.: Global burned area and biomass burning emissions
653 from small fires, *Journal of Geophysical Research: Biogeosciences*, 117, 2012.

654 Rogers, C. M. and Bowman, K. P.: Transport of smoke from the Central American fires of 1998, *Journal of*
655 *Geophysical Research: Atmospheres*, 106, 28357-28368, 2001.

656 Running, S., Q. Mu, M. Zhao. : MODIS/Terra Gross Primary Productivity 8-Day L4 Global 500m SIN Grid
657 V061, distributed by NASA EOSDIS Land Processes Distributed Active Archive Center,
658 <https://doi.org/10.5067/MODIS/MOD17A2H.061>. Accessed 2023-12, 2021.

659 Su, W., Charlock, T. P., And, F. G. R., and Rutan, D.: Photosynthetically active radiation from Clouds and the Earth's
660 Radiant Energy System (CERES) products, *Journal of Geophysical Research: Biogeosciences*, 2007.

661 Tosca, M., Randerson, J., Zender, C., Flanner, M., and Rasch, P. J.: Do biomass burning aerosols intensify drought in
662 equatorial Asia during El Nino?, *Atmospheric Chemistry and Physics*, 10, 3515-3528, 2010.

663 Tosca, M. G., Randerson, J. T., and Zender, C. S.: Global impact of smoke aerosols from landscape fires on climate
664 and the Hadley circulation, *Atmos Chem Phys*, 13, 5227-5241, 10.5194/acp-13-5227-2013, 2013.

665 van Marle, M. J. E., Kloster, S., Magi, B. I., Marlon, J. R., Daniau, A. L., Field, R. D., Arneth, A., Forrest, M., Hantson,
666 S., Kehrwald, N. M., Knorr, W., Lasslop, G., Li, F., Mangeon, S., Yue, C., Kaiser, J. W., and van der Werf, G. R.:
667 Historic global biomass burning emissions for CMIP6 (BB4CMIP) based on merging satellite observations with
668 proxies and fire models (1750-2015), *Geosci Model Dev*, 10, 3329-3357, 10.5194/gmd-10-3329-2017, 2017.

669 Veira, A., Lasslop, G., and Kloster, S.: Wildfires in a warmer climate: Emission fluxes, emission heights, and black
670 carbon concentrations in 2090–2099, *Journal of Geophysical Research: Atmospheres*, 121, 3195-3223, 2016.

671 Voulgarakis, A. and Field, R. D.: Fire influences on atmospheric composition, air quality and climate, *Current*
672 *Pollution Reports*, 1, 70-81, 2015.

673 Winker, D. M., Tackett, J. L., Getzewich, B. J., Liu, Z., Vaughan, M. A., and Rogers, R. R.: The global 3-D distribution
674 of tropospheric aerosols as characterized by CALIOP, *Atmos Chem Phys*, 13, 3345-3361, 10.5194/acp-13-3345-2013,
675 2013.

676 Yokelson, R., Urbanski, S., Atlas, E., Toohey, D., Alvarado, E., Crounse, J., Wennberg, P., Fisher, M., Wold, C., and
677 Campos, T.: Emissions from forest fires near Mexico City, *Atmos. Chem. Phys*, 7, 5569-5584, 2007.

678 Yokelson, R. J., Crounse, J., DeCarlo, P., Karl, T., Urbanski, S., Atlas, E., Campos, T., Shinozuka, Y., Kasputin, V.,
679 and Clarke, A.: Emissions from biomass burning in the Yucatan, *Atmospheric Chemistry and Physics*, 9, 5785, 2009.

680 Yue, S., Zhu, J., Chen, S., Xie, Q., Li, W., Li, L., Ren, H., Su, S., Li, P., and Ma, H.: Brown carbon from biomass
681 burning imposes strong circum-Arctic warming, *One Earth*, 5, 293-304, 2022.

682 Zhang, Y. W., Fan, J. W., Shrivastava, M., Homeyer, C. R., Wang, Y., and Seinfeld, J. H.: Notable impact of wildfires
683 in the western United States on weather hazards in the central United States, *P Natl Acad Sci USA*, 119, ARTN
684 e220732911910.1073/pnas.2207329119, 2022.

685 Zhong, Q. R., Schutgens, N., van der Werf, G., van Noije, T., Tsigaridis, K., Bauer, S. E., Mielonen, T., Kirkevåg, A.,
686 Seland, O., Kokkola, H., Checa-Garcia, R., Neubauer, D., Kipling, Z., Matsui, H., Ginoux, P., Takemura, T., Le Sager,
687 P., Remy, S., Bian, H. S., Chin, M., Zhang, K., Zhu, J. L., Tsyro, S. G., Curci, G., Protonotariou, A., Johnson, B.,
688 Penner, J. E., Bellouin, N., Skeie, R. B., and Myhre, G.: Satellite-based evaluation of AeroCom model bias in biomass
689 burning regions, *Atmos Chem Phys*, 22, 11009-11032, 10.5194/acp-22-11009-2022, 2022.

690